J. Fluid Mech. (2015), *vol.* 779, *pp.* 351–370.
doi:10.1017/jfm.2015.409

The asymptotic downstream flow of plane turbulent wall jets without external stream

Klaus Gersten†

Institute of Thermo- and Fluid Dynamics, Ruhr University, D-44801 Bochum, Germany

(Received 20 May 2013; revised 9 June 2015; accepted 13 July 2015;
first published online 17 August 2015)

The plane turbulent wall-jet flow without externally imposed stream is considered. It is assumed that the wall jet does not emerge from a second wall perpendicular to the velocity vector of the initial wall jet. The (kinematic) momentum flux $K(x)$ of the wall jet decreases downstream owing to the shear stress at the wall. This investigation is based on the hypothesis that the total friction force on the wall is smaller than the total inflow momentum flux. In other words, the turbulent wall jet tends to a turbulent 'half-free jet' with a non-zero momentum flux K_∞ ($\mathrm{m}^3\ \mathrm{s}^{-2}$) far downstream. The fact that the turbulent half-free jet is the asymptotic form of a turbulent wall jet is the basis for a singular perturbation method by which the wall-jet flow is determined. It turns out that the ratio between the wall distance y_m of the maximum velocity and the wall distance $y_{0.5}$ of half the maximum velocity decreases downstream to zero. Dimensional analysis leads immediately to a universal function of the dimensionless momentum flux $K(Re_x)/K_\infty$ that depends asymptotically only on the local Reynolds number $Re_x = \sqrt{(x-x_0)K_\infty}/\nu$, where x_0 denotes the coordinate of the virtual origin. When the values K and ν at the position $x - x_0$ are known, the asymptotic momentum flux K_∞ can be determined. Experimental data on all turbulent plane wall jets (except those emerging from a second plane wall) collapse to a single universal curve. Comparisons between available experimental data and the analysis make the hypothesis $K_\infty \neq 0$ plausible. A convincing verification, however, will be possible in the future, preferably by direct numerical simulations.

Key words: jets, shear layer turbulence, turbulent boundary layers

1. Introduction

The flow under consideration is the plane turbulent wall jet without externally imposed stream (figure 1). The flow is steady and incompressible. Numerous papers have dealt with the subject of turbulent wall jets. The review articles by Narasimha, Narayan & Parthasarathy (1973), Launder & Rodi (1981, 1983) and Schneider & Goldstein (1994) are worth mentioning. Unfortunately, not much can be found in the literature about the asymptotic downstream flow of turbulent wall jets. It appears that most authors hold the view that in this respect the turbulent wall jet behaves like a laminar wall jet. The latter tends to a flow with self-similar velocity distribution and vanishing jet momentum flux far downstream (cf. Schlichting & Gersten 2003, p. 180). However, it is overlooked that the asymptotic behaviour of the turbulent wall jet might be different from that of the laminar case.

† Email address for correspondence: K.Gersten@t-online.de

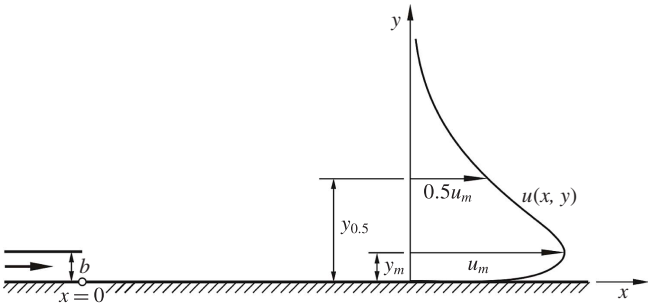

FIGURE 1. Geometry and notations of the plane wall jet.

Myers, Schauer & Eustis (1963) were presumably the first who treated the asymptotic behaviour of turbulent wall jets. They described the wall-jet flow by an integral method. They concluded that, far downstream, the time-averaged velocity is $u \sim (x - x_0)^{-1/2}$ and the half-maximum velocity distance is $y_{0.5} \sim (x - x_0)$. In other words, the wall jet tends to a turbulent half-free jet as limiting flow. As a consequence of this finding, the turbulent wall jet has a non-zero momentum flux far downstream. Furthermore, they found that the ratio $y_m/y_{0.5}$ (see figure 1) is not constant but rather a function of the streamwise coordinate x, tending to zero far downstream. The same result has been found by Hammond (1982) in his analysis. When the velocity distribution shown in figure 1 is depicted in non-dimensional form, i.e. $u/u_m = F(y/y_{0.5})$, the wall distance of the point of maximum velocity decreases in the downstream direction. Finally, the point of maximum velocity reaches the wall. Consequently, the velocity distribution is like that of a bisected free jet. Therefore the flow of the wall jet further upstream can be considered as a perturbation of the turbulent half-free jet flow.

Gersten & Herwig (1992, p. 753) treated the turbulent wall jet by a singular perturbation method. The problem is singular since the limiting solution (half-free jet) does not satisfy the no-slip condition at the wall. The perturbation analysis by Gersten & Herwig (1992) was limited to the first-order expansion and the theory was not compared with experimental results. In addition, and unfortunately, in the most important equation, the Greek letters κ and α got lost in the printing process. This motivated the present corrected and considerably extended paper.

As mentioned above, many authors hold the view that the momentum flux $K(x)$ tends to zero for $x \to \infty$. Examples of these authors are Narasimha *et al.* (1973), Wygnanski, Katz & Horev (1992), Schneider & Goldstein (1994) and George *et al.* (2000). Karlsson, Eriksson & Persson (1993), Abrahamsson, Johansson & Löfdahl (1994), George *et al.* (2000, cf. appendix B) and Barenblatt, Chorin & Prostokishin (2005) investigated wall jets emerging from a wall perpendicular to the velocity vector of the inflow. For this kind of wall jet the theory of the present paper is not valid. As Schneider (1985) has shown, the momentum flux of turbulent free jets emerging from orifices of plane walls decreases to zero far downstream. The same is, of course, true for a turbulent half-free jet. Therefore, wall jets emerging from a wall perpendicular to the inflow velocity vector have explicitly been excluded already in this investigation.

The basis of the following analysis is the hypothesis that the asymptotic momentum flux K_∞ is not equal to zero. In § 2 it is shown by dimensional analysis that one single curve in the representation $K/K_\infty = f(Re_x)$ is valid for all turbulent wall jets far downstream. The analysis is based on a four-layer structure described in § 3. For

known global functions $y_m(x)$, $y_{0.5}(x)$, $u_m(x)$ and $u_\tau(x)$, which quite frequently can be found as results of experimental investigations, the details of the flow field are given in § 4. Here, self-similar velocity distributions are assumed for each of the four layers separately. In § 5 it is shown how the universal asymptotic formula for K/K_∞ can be derived from the momentum-integral equation. In §§ 6–8 the four functions mentioned above are determined by a singular perturbation method. Finally, the theory is compared with experimental data in § 9.

2. Dimensional analysis (for $K_\infty \neq 0$)

The maximum velocity u_m of the turbulent wall jet with the asymptotic kinematic momentum flux K_∞ ($\mathrm{m}^3\ \mathrm{s}^{-2}$) has the form

$$u_m = f(x - x_0,\, \nu,\, K_\infty), \tag{2.1}$$

where x_0 is the coordinate of the virtual origin and ν the kinematic viscosity. The asymptotic formula (2.1) is by definition independent of the slot width b and the inlet momentum flux K_j.

Dimensional analysis leads to

$$\frac{u_m\, \nu}{K_\infty} = F(Re_x), \tag{2.2}$$

where the Reynolds number is defined as

$$Re_x = \frac{\sqrt{(x - x_0)\, K_\infty}}{\nu}. \tag{2.3}$$

The one and only curve in the representation of (2.2) is universal and valid for all possible plane turbulent wall jets.

Also the following dimensionless combinations can depend only on the Reynolds number:

$$\left.\begin{array}{llll} y_{0.5}/(x - x_0), & y_m/y_{0.5}\ \text{(figure 2)}, & u_m\, y_{0.5}/\nu\ \text{(figure 5)}, & \sqrt{(x - x_0)K}/\nu \\ Re_m = u_m\, y_m/\nu, & c_f/2 = \tau_w/\rho\, u_m^2\ \text{(figure 2)}, & \tau_w\, \nu^2/\rho\, K_\infty^2, & K/K_\infty\ \text{(figure 5)}, \end{array}\right\} \tag{2.4}$$

where K is the (kinematic) momentum flux (see definition in (4.14)), ρ the density, τ_w the wall shear stress, y_m the wall distance of the maximum velocity and $y_{0.5}$ the wall distance of the point with velocity $u_m/2$. All dimensionless combinations in (2.4) are also universal functions of Re_m (examples in figure 2).

3. Flow model

The flow field consists of two parts: (i) the lower part ($y < y_m$) behaves like a turbulent boundary layer; (ii) the upper part ($y > y_m$) behaves like a half-free jet. Similar to turbulent boundary layers the lower part of the wall jet can be divided into three layers: the viscous wall layer, the overlap layer and the so-called defect layer. Hence, the model of the wall-jet flow field under consideration has a four-layer structure. Furthermore it is assumed that the velocity distribution is self-similar, but separately in each of the four layers.

In many experimental investigations of turbulent wall jets the results focus on the global functions $y_m(x)$, $y_{0.5}(x)$, $u_m(x)$ and $u_\tau(x)$. In § 4 the flow field will be described in detail for the case that these four functions are given.

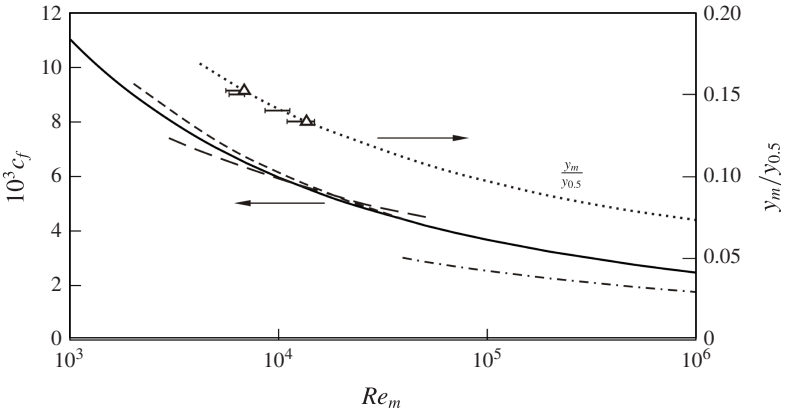

FIGURE 2. Skin friction law $c_f(Re_m)$ and thickness ratio $y_m/y_{0.5}$ for turbulent plane wall jets. —— after (4.28), - - - - after Hammond (1982), – – – after Launder & Rodi (1981), -·-·- asymptote, $G = 1$ in (4.28), · · · · · · after (6.1). Bars refer to experiments mentioned in table 1 presented in § 9; triangles are selected points for agreement with theory.

4. Flow field

4.1. *Asymptotic solution far downstream*

As already mentioned in the introduction, the turbulent wall-jet flow will be considered as a perturbation of the turbulent half-free jet flow. Turbulent free shear flows are slender, i.e. the mean local lateral velocity component is small compared to the dominant mean flow velocity. The flow spreads gradually, thus axial gradients are small in comparison to lateral gradients. These features allow the application of boundary-layer equations in place of the full Navier–Stokes equations (see Pope 2000, p. 111). Since the turbulent half-free jet flow is surrounded by quiescent fluid, the continuity equation and the momentum equation for the x-direction are

$$\frac{\partial u}{\partial x} + \frac{\partial v}{\partial y} = 0 \tag{4.1}$$

$$u\,\frac{\partial u}{\partial x} + v\,\frac{\partial u}{\partial y} = \frac{\partial}{\partial y}\left(\frac{\tau_t}{\rho}\right), \tag{4.2}$$

where τ_t is the turbulent shear stress. It is assumed that the velocity distribution of the turbulent half-free jet is self-similar:

$$u = U_N(x)\,\dot{F}(\tilde{\eta}). \tag{4.3}$$

In (4.3) the similarity variable is

$$\tilde{\eta} = k\,\frac{y}{y_{0.5}(x)}. \tag{4.4}$$

The dot in (4.3) refers to differentiation with respect to $\tilde{\eta}$. The constant k is defined by

$$\dot{F}(k) = \tfrac{1}{2}. \tag{4.5}$$

From the continuity equation (4.1) it follows that

$$v = -\frac{1}{k}\frac{\mathrm{d}(U_N y_{0.5})}{\mathrm{d}x} F + \frac{U_N}{k}\frac{\mathrm{d}y_{0.5}}{\mathrm{d}x}\tilde{\eta}\,\dot{F}. \tag{4.6}$$

The momentum equation (4.2) leads to the shear stress:

$$\frac{\tau_t}{\rho} = \frac{y_{0.5}}{k} U_N \frac{\mathrm{d}U_N}{\mathrm{d}x} F\dot{F} + \frac{2}{3}\frac{U_N}{k}\left(2y_{0.5}\frac{\mathrm{d}U_N}{\mathrm{d}x} + U_N\frac{\mathrm{d}y_{0.5}}{\mathrm{d}x}\right) F^3. \tag{4.7}$$

Dimensional analysis requires that $y_{0.5}$ is proportional to $x - x_0$, where x_0 is the coordinate of the virtual origin of the half-free jet:

$$y_{0.5} = 4\alpha k(x - x_0). \tag{4.8}$$

The rate of spreading of the half-free jet is $4\alpha k$, and α is a slenderness parameter.

As will be mentioned later, several turbulence models applied to turbulent free jets can be found in the literature. In the turbulence model used here it is assumed that the eddy viscosity ν_t is independent of $\tilde{\eta}$ (see Pope 2000, p. 137).

Dimensional analysis then yields the ansatz

$$\nu_t(x) = \frac{\alpha}{k} U_N(x)\, y_{0.5}(x). \tag{4.9}$$

Therefore it follows for the shear stress that

$$\frac{\tau_t}{\rho} = k\frac{\nu_t}{y_{0.5}}\frac{\partial u}{\partial\tilde{\eta}} = \alpha\, U_N^2(x)\,\ddot{F}(\tilde{\eta}). \tag{4.10}$$

Combination of (4.7) and (4.10) leads to a differential equation for the function $F(\tilde{\eta})$. With $U_N(x) \sim (x - x_0)^{-1/2}$ the following ordinary differential equation results:

$$\ddot{F} + 2F\dot{F} = 0, \tag{4.11}$$

because the factor in front of F^3 in (4.7) vanishes.

The boundary conditions for $F(\tilde{\eta})$ are

$$\left.\begin{array}{lll} \tilde{\eta} = 0\text{:}\ F = 0, & \dot{F} = 1, & \ddot{F} = 0 \\ \tilde{\eta} \to \infty\text{:}\ F = 1, & \dot{F} = 0, & \ddot{F} = 0. \end{array}\right\} \tag{4.12}$$

The solution of (4.11) is

$$F = \tanh\tilde{\eta}, \quad \dot{F} = 1 - (\tanh\tilde{\eta})^2\,. \tag{4.13a,b}$$

A comparison of this solution with experimental results will be discussed later in § 4.5.

The momentum flux

$$K(x) = \int_0^\infty u^2(x, y)\,\mathrm{d}y \tag{4.14}$$

can now be determined for the turbulent half-free jet:

$$K_\infty = \tfrac{8}{3}\alpha\,(x - x_0)\,U_N^2(x), \tag{4.15}$$

which is independent of x. This leads to the formula

$$U_N(x) = \sqrt{\frac{3\,K_\infty}{8\alpha\,(x - x_0)}}. \tag{4.16}$$

The turbulence model expressed by (4.9) has been chosen here because of the simple solution for the velocity distribution $\dot{F}(\tilde{\eta})$. Solutions for turbulent free jet flows with alternative turbulence modelling can also be found in the literature, for example Tollmien (1926), Saffman (1970), Schneider & Mörwald (1987) and Schneider (1991). These solutions lead to different differential equations for $F(\tilde{\eta})$ and, hence, to different constants in (4.16). However, the hypothesis $K_\infty \neq 0$ proposed here would not be affected by the choice of the turbulence model for the half-free jet flow.

4.2. *Viscous wall layer*

In this case results for the viscous wall layer of turbulent boundary layers can be adopted, see Schlichting & Gersten (2003, pp. 572, 523). The x-component of the velocity is given by the universal distribution

$$u^+(y^+) = \frac{u(x, y)}{u_\tau(x)} = F(y^+) \tag{4.17}$$

where

$$y^+ = \frac{y\,u_\tau}{\nu} \tag{4.18}$$

and

$$u_\tau(x) = \sqrt{\frac{\tau_w}{\rho}}. \tag{4.19}$$

The limiting form of the function $F(y^+)$ is

$$\lim_{y^+ \to \infty} u^+(y^+) = \frac{1}{\kappa} \ln y^+ + C^+ \tag{4.20}$$

where κ is called the Kármán constant and C^+ is a further universal constant, determined from numerous experiments to be $C^+ = 5.0$ for smooth walls. In the literature, (4.20) is denoted as the 'logarithmic law of the wall'. For high Reynolds numbers the y-component of the velocity vanishes in the viscous wall layer, and the shear stress $\tau(x)$ is independent of y^+ and, hence, equal to the wall shear stress $\tau_w(x)$, see Schlichting & Gersten (2003, p. 573). An analytic description of the universal function $F(y^+)$ is given in Schlichting & Gersten (2003, p. 524).

4.3. *Overlap layer*

The wall layer ($y \leqslant y_m$) of turbulent wall jets has the same three-layer structure as turbulent boundary layers. These layers are the viscous wall layer, the so-called defect layer ($0 \leqslant y \leqslant y_m$) and the overlap layer in between. The latter is part of the viscous wall layer and hence independent of y_m, as well as part of the defect layer and hence independent of the kinematic viscosity ν. Therefore the gradient of the velocity u^+ in the overlap layer is independent of ν and y_m.

Hence, the matching condition for the velocity gradient reads as follows:

$$\lim_{\eta\to 0}\eta\frac{\partial u^+}{\partial \eta}=\lim_{y^+\to\infty}y^+\frac{\partial u^+}{\partial y^+}=\frac{1}{\kappa}, \tag{4.21}$$

where

$$\eta=\frac{y}{y_m} \tag{4.22}$$

is the dimensionless distance from the wall. Integrating the wall-layer part in (4.21) leads to (4.20). Integrating the defect-layer part in (4.21) leads to

$$\lim_{\eta\to 0}u^+(\eta)=\frac{u_m}{u_\tau}+\frac{1}{\kappa}\ln\eta-\bar{C}, \tag{4.23}$$

where the integration constant is defined as

$$\bar{C}=\lim_{\eta\to 0}\int_\eta^1\left(\frac{\mathrm{d}u^+}{\mathrm{d}\eta}-\frac{1}{\kappa\eta}\right)\mathrm{d}\eta. \tag{4.24}$$

The matching condition for the velocity u^+ in the overlap layer reads as follows:

$$\frac{u_m}{u_\tau}-\bar{C}+\frac{1}{\kappa}\ln\eta=\frac{1}{\kappa}\ln y^+ + C^+ \tag{4.25}$$

or

$$\frac{1}{\gamma}=\frac{1}{\kappa}\ln(\gamma\, Re_m)+C^+ +\bar{C} \tag{4.26}$$

with

$$\gamma=\frac{u_\tau}{u_m}=\sqrt{\frac{c_f}{2}},\quad Re_m=\frac{u_m\, y_m}{\nu}. \tag{4.27a,b}$$

This implicit friction law $c_f=f(Re_m)$ can be written in explicit form as

$$\sqrt{\frac{c_f}{2}}=\gamma=\frac{\kappa}{\ln Re_m}\,G(\Lambda_m;\ D_m,\ E_m) \tag{4.28}$$

where

$$\Lambda_m=2\ln Re_m \tag{4.29}$$

$$D_m=2\,[\ln(2\kappa)+\kappa\,(C^+ +\bar{C})]=2.036 \tag{4.30}$$

$$E_m=0. \tag{4.31}$$

The function $G(\Lambda;\ D,\ E)$ has been defined and tabulated by Gersten & Herwig (1992). More details are given in appendix A. The friction law according to (4.28) is shown in figure 2. The agreement with experimental data by Launder & Rodi (1981) and Hammond (1982) is very good. As will become apparent later, the limits $Re_m\to\infty$ and $\gamma\to 0$ are equivalent to the limits $x\to\infty$ and $Re_x\to\infty$, respectively.

The dotted line in figure 2 will be discussed in § 9.

4.4. *Defect layer* $(0 < y \leqslant y_m)$

4.4.1. *Flow field*

In the limiting case of infinite Reynolds number (which is equivalent to $y_m/y_{0.5} \to 0$), the velocity $u(x, y)$ in the defect layer attains the value $u_m(x)$. Therefore it seems natural to write the velocity in the form of a defect law

$$u(x, \eta) = u_m(x) - u_\tau(x) f'(\eta) \tag{4.32}$$

with

$$\eta = \frac{y}{y_m}. \tag{4.33}$$

The continuity equation (4.1) leads to

$$v(x, \eta) = \frac{\mathrm{d}y_m}{\mathrm{d}x} u_\tau \left(f - \eta f'\right) + y_m \frac{\mathrm{d}u_\tau}{\mathrm{d}x} f - y_m \frac{\mathrm{d}u_m}{\mathrm{d}x} \eta. \tag{4.34}$$

When the velocity components are known, the shear stress can be determined by using the momentum equation (4.2). Transforming (4.2) into the x, η coordinate system and using (4.32) leads to

$$y_m u_m \frac{\mathrm{d}u_m}{\mathrm{d}x} + u_\tau^2 \left(A\eta f'' + B f' + C f'^2 + D f f''\right) = \frac{\partial}{\partial \eta}\left(\frac{\tau_t}{\rho}\right) \tag{4.35}$$

where

$$\left.\begin{aligned} A(x) &= \frac{1}{u_\tau} \frac{\mathrm{d}\,(y_m u_m)}{\mathrm{d}x}, \quad B(x) = -\frac{y_m}{u_\tau^2} \frac{\mathrm{d}(u_\tau u_m)}{\mathrm{d}x}, \\ C(x) &= \frac{y_m}{u_\tau} \frac{\mathrm{d}u_\tau}{\mathrm{d}x}, \quad D(x) = -\frac{1}{u_\tau} \frac{\mathrm{d}(u_\tau y_m)}{\mathrm{d}x}, \end{aligned}\right\} \tag{4.36a–d}$$

see Schlichting & Gersten (2003, p. 574).

Splitting the shear stress into two parts

$$\frac{\tau_t(x, \eta)}{\rho} = y_m u_m \frac{\mathrm{d}u_m}{\mathrm{d}x} \eta + u_\tau^2 s(x, \eta) \tag{4.37}$$

reduces the momentum equation (4.35) to

$$A\eta f'' + B f' + C f'^2 + D f f'' = s'. \tag{4.38}$$

The term s' refers to differentiating $s(x, \eta)$ with respect to η.

Using the condition $s(x, 0) = 1$, integration of (4.38) leads to

$$s(x, \eta) = 1 + A\left(\eta f' - f\right) + B f + C \int_0^\eta f'^2 \,\mathrm{d}\eta + D \int_0^\eta f f'' \,\mathrm{d}\eta. \tag{4.39}$$

4.4.2. *Determination of the function* $f(\eta)$

The function $f(\eta)$ represents the self-similarity of the velocity distribution in the defect layer according to (4.32). This function must satisfy the differential equation (4.38), which in this case must be independent of x. This means that A and B in (4.38) must be constants, whereas C and D will become negligibly small and $s(\eta)$ depends only on η.

Now one should keep in mind that the defect layer of turbulent wall jets behaves like the defect layer of turbulent equilibrium boundary layers. The latter are defined by the self-similarity of the velocity distribution, see Schlichting & Gersten (2003, p. 580). For turbulent equilibrium boundary layers the functions $A(x)$ and $B(x)$ are constant for high Reynolds numbers. It is therefore appropriate to assume the analogous behaviour for the wall jet in the limit $Re_x \to \infty$:

$$A(Re_x \to \infty) = A_\infty \quad B(Re_x \to \infty) = B_\infty, \tag{4.40a,b}$$

which will be verified in (4.47) after the following lines of formulae.

Introducing the characteristic length

$$\tilde{\Delta}(x) = \frac{u_m\, y_m}{u_\tau} \tag{4.41}$$

leads to

$$\left.\begin{aligned} A(x) &= \frac{\mathrm{d}\tilde{\Delta}}{\mathrm{d}x} + \frac{\tilde{\Delta}}{u_\tau}\frac{\mathrm{d}u_\tau}{\mathrm{d}x}, \quad B(x) = -\left(\frac{\tilde{\Delta}}{u_m}\frac{\mathrm{d}u_m}{\mathrm{d}x} + \frac{\tilde{\Delta}}{u_\tau}\frac{\mathrm{d}u_\tau}{\mathrm{d}x}\right) \\ C(x) &= \gamma\,\frac{\tilde{\Delta}}{u_\tau}\frac{\mathrm{d}u_\tau}{\mathrm{d}x}, \quad D(x) = -\gamma\left(A(x) + \frac{\tilde{\Delta}}{\gamma}\frac{\mathrm{d}\gamma}{\mathrm{d}x}\right). \end{aligned}\right\} \tag{4.42a–d}$$

From the definition of γ in (4.27*a*) it follows that

$$\frac{\tilde{\Delta}}{u_\tau}\frac{\mathrm{d}u_\tau}{\mathrm{d}x} = \frac{\tilde{\Delta}}{u_m}\frac{\mathrm{d}u_m}{\mathrm{d}x} + \frac{\tilde{\Delta}}{\gamma}\frac{\mathrm{d}\gamma}{\mathrm{d}x}. \tag{4.43}$$

Differentiation of (4.26) with respect to x leads to

$$\frac{\tilde{\Delta}}{\gamma}\frac{\mathrm{d}\gamma}{\mathrm{d}x} = -\frac{A(x)}{\kappa}\,\gamma + O(\gamma^2). \tag{4.44}$$

For the limit $\gamma \to 0$ the terms proportional to $\mathrm{d}\gamma/\mathrm{d}x$ in (4.42*a–d*) and (4.43) are small compared to the other terms and can be neglected. In the flow far downstream $u_m(x)$ changes into $U_N(x)$ according to (4.16). From (4.42*b*) and (4.43) it follows that

$$\frac{\tilde{\Delta}}{u_m}\frac{\mathrm{d}u_m}{\mathrm{d}x} = \frac{\tilde{\Delta}}{U_N}\frac{\mathrm{d}U_N}{\mathrm{d}x} = -\frac{\tilde{\Delta}(x)}{2\ (x - x_0)} = -\frac{B_\infty}{2}. \tag{4.45}$$

Therefore $\tilde{\Delta}(x)$ is proportional to $x - x_0$ or to $y_{0.5}(x)$ according to (4.8):

$$\tilde{\Delta}(x) = A_1\, y_{0.5}(x) = 4\alpha k A_1\ (x - x_0). \tag{4.46}$$

The limiting constant $A_\infty = A(x \to \infty)$ reads as follows:

$$A_\infty = \frac{B_\infty}{2} = 2\alpha k A_1 \tag{4.47}$$

and, hence, equation (4.44) reduces to

$$\frac{\mathrm{d}\gamma}{\mathrm{d}x} = -\frac{\gamma^2}{2\kappa\ (x - x_0)} + O(\gamma^3), \tag{4.48}$$

which after integration leads to

$$\gamma = \frac{\kappa}{\ln Re_x}\,[1 + o(1)], \tag{4.49}$$

where Re_x is defined in (2.3). This formula shows clearly that the limit $Re_x \to \infty$ is equivalent to the limit $\gamma \to 0$. Combining (4.41) and (4.46) leads to

$$\frac{y_m}{y_{0.5}} = A_1 \frac{u_\tau}{u_m} = A_1\,\gamma. \tag{4.50}$$

The ratio $y_m/y_{0.5}$ tends to zero far downstream, as has been anticipated in the present hypothesis for $K_\infty \neq 0$.

In § 6 equation (4.50) will be extended to an asymptotic series expansion (6.1). By using this extension it can be shown that the functions $A(x)$ and $B(x)$ have for $\gamma \to 0$ the following asymptotic form:

$$A(x) = A_\infty + O(\gamma), \quad B(x) = B_\infty + O(\gamma). \tag{4.51a,b}$$

The function $f(\eta)$ has to satisfy the following ordinary differential equation, which results from (4.39) for the limit $x \to \infty$:

$$s(\eta) = 1 + A_\infty\,(\eta f' - f) + B_\infty f. \tag{4.52}$$

In order to enable the solution of the ordinary differential equation (4.52), a turbulence model is needed that provides a relation between $f(\eta)$ and $s(\eta)$. Instead of that, an indirect turbulence model will be applied here. A plausible function $f(\eta)$ will be chosen and the corresponding function $s(\eta)$ can then be determined from (4.52).

The function $f(\eta)$ must satisfy the following boundary conditions:

$$\eta = 1\text{: } f = f_m, \quad f' = 0, \quad f'' = 0, \quad f''' = 0 \tag{4.53}$$

$$\eta \to 0\text{: } f = 0, \quad f' = \bar{C} - \frac{1}{\kappa}\ln\eta, \quad f'' = -\frac{1}{\kappa\eta}. \tag{4.54}$$

For $\eta \to 0$ the condition $f = 0$ follows from (4.34) for $v(x, \eta \to 0) = 0$; the conditions for f' and f'' have been derived in (4.23).

In particular the physical significance of the integration constant $\bar{C}$ is apparent in (4.24). The condition $f'''(\eta = 1) = 0$ results from 'patching' the term $\partial^2 u/\partial y^2$ of the defect layer and the outer layer at $y = y_m$ (see (4.63)).

For $\eta = 1$ the value f_m is a measure of $v(x, \eta = 1)$, and the conditions $f' = 0$ and $f'' = 0$ result from $u = u_m$.

The following function consisting of a logarithmic term and a power series satisfies all boundary conditions appearing in (4.53) and (4.54):

$$f'(\eta) = \frac{1}{\kappa}\left(-\ln\eta - \frac{5}{6} + \frac{3}{2}\eta^2 - \frac{2}{3}\eta^3\right) \tag{4.55}$$

with

$$\kappa = 0.41, \quad \bar{C} = -\frac{5}{6\kappa} = -2.033, \quad f_m = \frac{1}{2\kappa} = 1.220. \tag{4.56a–c}$$

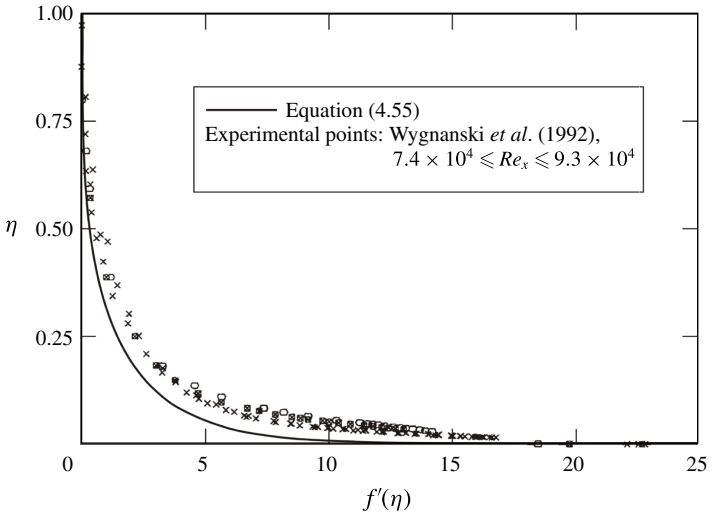

FIGURE 3. Self-similar distribution of the defect velocity in the defect layer.

In figure 3 the defect velocity

$$\frac{u_m - u}{u_\tau} = f'(\eta) \tag{4.57}$$

is compared with experimental data of Wygnanski *et al.* (1992). The difference between theory and experiment may be attributed to the fact that the experiments refer to fairly low Reynolds numbers. The maximum of the absolute difference for $f'(\eta) = 5$ is about $\Delta y = 0.2$ mm, which is surprisingly small. The theoretical curve $f'(\eta)$ does not depend on any empirical constant. It is proportional to $1/\kappa$ according to (4.55), where κ is the well-defined ((4.21), $Re \to \infty$, zero pressure gradient) universal Kármán constant $\kappa = 0.41$.

4.5. *Outer layer* ($y \geqslant y_m$)

It is assumed that the distribution of the velocity is again self-similar:

$$u = u_m(x)\, \dot{F}(\bar{\eta}) \tag{4.58}$$

where the similarity variable is

$$\bar{\eta} = \frac{y - y_m(x)}{\Delta(x)} \tag{4.59}$$

with

$$\Delta(x) = \frac{y_{0.5} - y_m}{k}. \tag{4.60}$$

The dot designates differentiation with respect to $\bar{\eta}$. The variable $\bar{\eta}$ is a generalization of the variable $\tilde{\eta}$ in (4.4) for $y_m \neq 0$.

From the continuity equation it follows that

$$v = -\frac{\mathrm{d}(u_m \Delta)}{\mathrm{d}x} F + u_m \frac{\mathrm{d}y_m}{\mathrm{d}x} \dot{F} + u_m \frac{\mathrm{d}\Delta}{\mathrm{d}x} \bar{\eta}\, \dot{F} + \frac{\mathrm{d}(y_m\, u_\tau)}{\mathrm{d}x} f_m - \frac{\mathrm{d}(y_m\, u_m)}{\mathrm{d}x}. \tag{4.61}$$

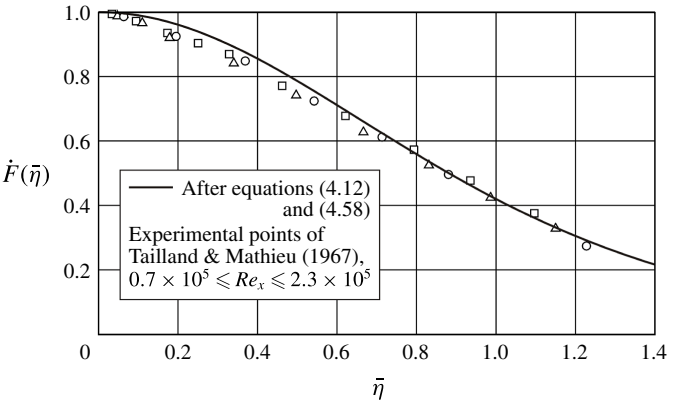

FIGURE 4. Self-similar velocity distribution in the outer layer.

The momentum equation leads to the shear stress:

$$\frac{\tau_t}{\rho} = u_m \Delta \frac{\mathrm{d}u_m}{\mathrm{d}x} F \dot{F} + \frac{2}{3} u_m \left(2\Delta \frac{\mathrm{d}u_m}{\mathrm{d}x} + u_m \frac{\mathrm{d}\Delta}{\mathrm{d}x} \right) F^3 + \left[\frac{\mathrm{d}(y_m u_\tau)}{\mathrm{d}x} f_m - \frac{\mathrm{d}(y_m u_m)}{\mathrm{d}x} \right] u_m \dot{F} + u_\tau^2 + \frac{\mathrm{d}(y_m u_m^2)}{\mathrm{d}x} - \left[u_\tau \frac{\mathrm{d}(y_m u_m)}{\mathrm{d}x} + y_m \frac{\mathrm{d}(u_\tau u_m)}{\mathrm{d}x} + u_m \frac{\mathrm{d}(y_m u_\tau)}{\mathrm{d}x} \right] f_m. \tag{4.62}$$

Equations (4.61) and (4.62) reduce to (4.6) and (4.7) for the limit $x \to \infty$, when $y_m \to 0$, $u_m \to U_N(x)$ and $\Delta \to y_{0.5}/k$ are taken into account.

At $y = y_m$ the values for u, $\partial u/\partial y$, v and τ_t/ρ for the defect layer ($\eta = 1$) and the outer layer ($\bar{\eta} = 0$) are equal ('patching'). For $\partial^2 u/\partial y^2$ the patching condition is as follows:

$$f'''(\eta = 1) = 2 \left[\frac{k A_1}{1 - A_1 \gamma} \right]^2 \gamma. \tag{4.63}$$

In the limit $\gamma \to 0$ it follows that $f'''(1) = 0$ in (4.53).

The function $F(\bar{\eta})$ is identical with $F(\tilde{\eta})$. All results for $F(\tilde{\eta})$ in § 4.1 can be used in this generalization. Figure 4 shows the comparison of the solution for the outer layer with experimental results of Tailland & Mathieu (1967).

4.6. *Determination of the momentum flux $K(x)$*

The momentum flux

$$K(x) = \int_0^\infty u^2(x, y)\, \mathrm{d}y \tag{4.64}$$

can now be determined if (4.32) and (4.58) are used for the integration. The result is

$$K(x) = 0.756\, u_m^2\, y_{0.5} \left(1 + 0.322 \frac{y_m}{y_{0.5}} - 2.644 f_m \sqrt{\frac{c_f}{2}} \frac{y_m}{y_{0.5}} \right). \tag{4.65}$$

The constants are

$$0.756 = \frac{2}{3k}, \quad 0.322 = \frac{3k}{2} - 1, \quad 2.644 = 3k, \quad k = 0.8814. \tag{4.66a–d}$$

The formula (4.65) can be used to determine the momentum flux K when the global values in the formula are known.

5. Momentum-integral equation

The momentum flux $K(x)$ must satisfy the momentum-integral equation:

$$K(x) = K_\infty + \int_x^\infty \frac{\tau_w}{\rho}\,\mathrm{d}x. \tag{5.1}$$

A dimensionless friction velocity

$$\gamma_G(x) = \frac{u_\tau(x)}{U_N(x)} \tag{5.2}$$

is introduced, where $U_N(x)$ is given in (4.16). Then (5.1) can be written as

$$\frac{K(x)}{K_\infty} = 1 + \frac{3}{8\alpha}\int_x^\infty \frac{\gamma_G^2(x)\,\mathrm{d}x}{x - x_o} = 1 + \frac{3}{4\alpha}\int_\Lambda^\infty \gamma_G^2(\Lambda)\,\mathrm{d}\Lambda, \tag{5.3}$$

where

$$\Lambda = \ln Re_x = \ln\left(\sqrt{K_\infty (x - x_o)}/\nu\right). \tag{5.4}$$

The integration leads to the final formula (see appendix A):

$$\frac{K(\Lambda)}{K_\infty} = 1 + \frac{3\kappa^2}{4\alpha}\left\{\frac{\gamma_G(\Lambda)}{\kappa} + \left[\frac{\gamma_G(\Lambda)}{\kappa}\right]^2 + O\left(\frac{1}{\Lambda^3}\right)\right\}. \tag{5.5}$$

(This equation without the term $O(\gamma_G^2)$ appears also in Gersten & Herwig (1992) and in Schlichting & Gersten (2003). Unfortunately, there the Greek letters κ and α got lost in the printing process.)

6. Wall-jet flow described by perturbation method

So far the flow field of the wall jet has been described for given functions $y_m(x)$, $y_{0.5}(x)$, $u_m(x)$ and $u_\tau(x)$. These functions are known in the limiting case $x \to \infty$, see § 4.1. Now, for the general case, these functions will be described by a perturbation method. From (5.5) it is obvious to use γ_G as the perturbation parameter. The following power series expansions will be applied (with respect to A_1 see (4.50)):

$$\frac{y_m}{y_{0.5}} = A_1\,\gamma_G\,(1 + A_2\,\gamma_G + \cdots) \tag{6.1}$$

$$\frac{u_m}{U_N} = 1 + B_1\,\gamma_G + B_2\,\gamma_G^2 + \cdots. \tag{6.2}$$

It is assumed that the asymptotic formula (see (4.8))

$$y_{0.5} = 4\alpha k(x - x_0) \tag{6.3}$$

is generally valid, which is in accordance with experiments. Introducing (6.1) and (6.2) into (4.27) yields

$$\gamma = \gamma_G \frac{U_N}{u_m}, \quad Re_m = \frac{u_m}{U_N}\frac{y_m}{y_{0.5}} P\, Re_x, \tag{6.4a,b}$$

where

$$P = k\sqrt{6\alpha}. \tag{6.5}$$

The skin friction law (4.26) is now transformed into

$$\frac{1}{\gamma_G} = \frac{1}{\kappa}\ln\left(\gamma_G^2 Re_x\right) + \hat{D} + \hat{E}\,\gamma_G \tag{6.6}$$

with

$$\hat{D} = \frac{1}{\kappa}\ln(A_1 P) - B_1 + C^+ + \bar{C}, \quad \hat{E} = \frac{1}{\kappa}A_2 - B_2. \tag{6.7a,b}$$

In appendix A it is shown that the explicit solution of (6.6) is

$$\gamma_G = \frac{\kappa}{\ln Re_x} G(\Lambda;\ D,\ E) \tag{6.8}$$

where

$$\Lambda = \ln Re_x, \quad D = 2\ln\kappa + \kappa\,\hat{D}, \quad E = \kappa^2\,\hat{E}. \tag{6.9a–c}$$

7. Determination of the universal constants

It is desirable to determine the universal constants α, A_1, A_2, B_1 and B_2 defined in (4.8), (6.1) and (6.2) in such a way that the analysis is optimally concordant with existing experiments. Unfortunately, all existing experimental data on plane turbulent wall jets belong to rather low Reynolds numbers and, hence, are far away from the asymptotic state. Despite this deficiency, matching of the analysis with experimental data will be attempted.

Experimental results on six available turbulent wall-jet flows have been analysed. The main global values are listed in table 1 below. The constant α $(= \mathrm{d}y_{0.5}/\mathrm{d}x/(4k))$ introduced in (4.8) can be taken from Launder & Rodi (1981), who analysed about 20 experimental investigations. They found $\alpha = 0.021$. This is in accordance with the mean value resulting from the experiments in the table (k from (4.66*d*)):

$$\alpha = 0.021, \quad P = k\sqrt{6\alpha} = 0.3129. \tag{7.1a,b}$$

Taking into account (4.16), (6.1) and (6.2) and comparing (5.5) and (4.65) provide the following two conditions that the constants A_1, A_2, B_1 and B_2 must satisfy:

$$0.322\,A_1 + 2\,B_1 = \frac{3\kappa}{4\alpha} \tag{7.2}$$

$$A_1\,(0.644\,B_1 - 2.644\,f_m) + B_1^2 + 2\,B_2 + 0.322\,A_1\,A_2 = \frac{3}{4\alpha}. \tag{7.3}$$

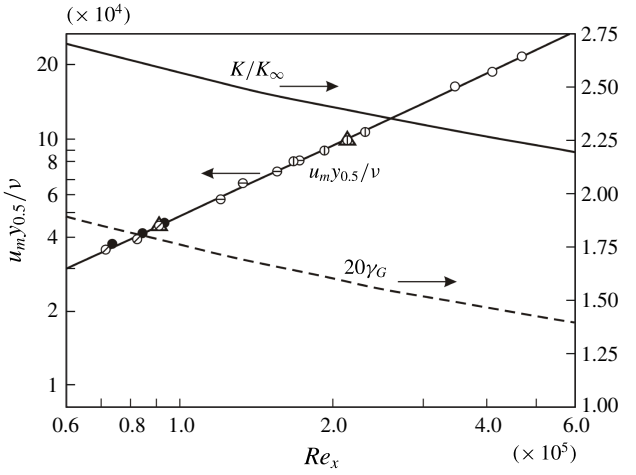

FIGURE 5. Universal functions. K/K_∞ according to (5.5) and (6.6), $u_m\, y_{0.5}/\nu = Re_m\, y_{0.5}/y_m$, Re_m and γ according to (6.4), γ_G according to (6.6). Experiments: see table 1 for symbols. Δ denotes selected points for agreement with theory.

Two still missing relations between the constants follow from the condition that the experimental values of two particular wall-jet velocity profiles should coincide with the corresponding theoretical values. The following two points have been selected for the agreement with the theory:

Point I (from Tailland & Mathieu 3, $x - x_0 = 1.06$ m)

$$\frac{y_m}{y_{0.5}} = 0.155, \quad \frac{u_m\, y_{0.5}}{\nu} = 0.447 \times 10^5. \tag{7.4a,b}$$

Point II (from Tailland & Mathieu 1, $x - x_0 = 1.05$ m)

$$\frac{y_m}{y_{0.5}} = 0.131, \quad \frac{u_m\, y_{0.5}}{\nu} = 1.003 \times 10^5. \tag{7.5a,b}$$

In addition to (7.2) and (7.3), the (6.1) and (6.2) specified for each of these points lead finally to six nonlinear algebraic equations for A_1, A_2, B_1, B_2, γ_{GI} and γ_{GII}. The results are the universal constants:

$$A_1 = 1.4798, \quad A_2 = 1.7441, \quad B_1 = 7.1002, \quad B_2 = -8.7227. \tag{7.6a–d}$$

The positions of the points are given by:

$$\left.\begin{aligned} \gamma_{GI} &= 0.08923 \;\; (Re_x = 0.9091 \times 10^5, \;\; Re_m = 6789) \\ \gamma_{GII} &= 0.07944 \;\; (Re_x = 2.1287 \times 10^5, \;\; Re_m = 13\,451). \end{aligned}\right\} \tag{7.7}$$

The two selected points I and II are marked in figures 2 and 5 by triangles.

The numerical values of the universal constants should be considered preliminary until experimental data for higher Reynolds numbers become available.

https://doi.org/10.1017/jfm.2015.409 Published online by Cambridge University Press

Symbol	Authors (year)	$Re_j = U_j\, b/\nu$	Slot width b (mm)	Kinematic viscosity ν ($\times 10^5$ m^2 s^{-1})	Range of x/b	Thickness slope ($\mathrm{d}y_{0.5}/\mathrm{d}x$)	Virtual origin x_o (m)	Thickness ratio $y_m/y_{0.5}$	Inlet jet momentum K_j (m^3 s^{-2})	Asymptotic momentum $\bar{K}_\infty$ (m^3 s^{-2})
○	Myers *et al.* (1963)	56 500	12.7	1.5	100–180	0.075	−0.085		56.6	20.7
◐	Tailland & Mathieu 1 (1967)	25 000	6	1.44	100–200	0.070	−0.050	0.13	21.6	9.0
●	Wygnanski *et al.* (1992)	19 000	5	1.5	60–100	0.075	−0.050	0.15	16.3	3.5
⊖	Tailland & Mathieu 2 (1967)	18 000	6	1.44	100–200	0.079	−0.001	0.14	11.2	5.0
⊘	Tailland & Mathieu 3 (1967)	11 000	6	1.46	100–200	0.077	−0.060	0.16	4.3	1.7
⊕	Bradshaw & Gee (1960)	6 080	0.46	1.49	793–1224	0.073	0		18.0	3.4

TABLE 1. Experimental data.

8. Determination of the asymptotic momentum flux K_∞

When the values u_m, $y_{0.5}$ and ν at the position $x - x_0$ are known, the asymptotic momentum flux K_∞ can be determined by using the universal function shown in figure 5. The combination $u_m\, y_{0.5}/\nu$ leads to the corresponding value Re_x and, via (2.3), to K_∞. All positions x in a particular wall jet should lead to the same value K_∞. This would be true to a greater extent the further downstream the positions are. The mean value $\bar{K}_\infty$ of all analysed profiles of a particular wall jet is considered as the asymptotic momentum flux of this wall jet.

When the values K and ν at the position $x - x_0$ are known K_∞ can be determined by using the universal function for $K(Re_x)/K_\infty$, also shown in figure 5. Here an iteration process would lead to the solution K_∞.

9. Comparisons with experiments

Six turbulent wall jets documented in the literature have been analysed. The $\bar{K}_\infty$-values and other characteristic parameters are listed in table 1. The values $u_m\, y_{0.5}/\nu$ of the analysed wall jets are in good agreement with the theoretical universal curve in figure 5. The experimental results by Bradshaw & Gee (1960) are not shown in figure 5 because they are practically identical with the results by Tailland & Mathieu 3 (1967). The universal relation between $K/\bar{K}_\infty$ and Re_x is also shown in figure 5.

The experimental data for the thickness ratio $y_m/y_{0.5}$ are given in table 1 for four wall jets. They are compared with the present theory in figure 2. The short bars refer to the values of $y_m/y_{0.5}$ according to the table averaged over the covered range of Reynolds numbers Re_m. The authors obviously assumed that the thickness ratio is a constant for the entire wall jet. The analysis of this paper, however, shows that $y_m/y_{0.5}$ decreases monotonically with increasing Re_m. The dotted line in figure 2 corresponds to (6.1). It is a necessary condition for the hypothesis $K_\infty \neq 0$ that $y_m/y_{0.5}$ tends to zero for $Re_m \to \infty$ (see u/u_m in figure 6).

The ratio of K_∞/K_j is not a universal constant, but it varies in the table between 0.19 and 0.45. It depends mainly on the velocity distribution at the inflow. Narasimha *et al.* (1973) have non-dimensionalized $x - x_0$ by K_j rather than by K_∞ as has been done in the present investigation. Asymptotic formulae should not depend on K_j.

In figure 6 the theoretical distributions of the axial velocity and the shear stress are compared with experimental data of Tailland & Mathieu (1967). The corresponding formulae (valid for all turbulent wall jets) are

$$\frac{u}{u_m} = 1 - (\gamma_G - 7.10\,\gamma_G^2) f'(\eta) \quad \eta = \frac{y}{y_m} \leqslant 1 \tag{9.1}$$

$$\frac{u}{u_m} = \dot{F}(\bar{\eta}) \quad \bar{\eta} = 0.8814\,\frac{y - y_m}{y_{0.5} - y_m} \geqslant 0 \tag{9.2}$$

$$\frac{\tau_t}{\rho\, U_N^2} = -0.0548\eta\gamma_G + [1 + 0.0548\,(\eta f' + f) - 0.8734\eta]\gamma_G^2 \quad 0 < \eta \leqslant 1 \tag{9.3}$$

$$\begin{aligned}\frac{\tau_t}{\rho\, U_N^2} \;=\; & 0.021\,\ddot{F} + [0.534\,\ddot{F} - 0.0548\,\dot{F}]\,\gamma_G \\ & + [0.757\,\ddot{F} - 0.866\,(F^3 - 1) - 0.673\,\dot{F}]\,\gamma_G^2 \quad \bar{\eta} \geqslant 0.\end{aligned} \tag{9.4}$$

It should be emphasized that the limiting solution does not satisfy the no-slip condition at the wall and has zero wall shear stress. The solution including the first-order disturbances satisfies the no-slip condition, but still has zero wall shear

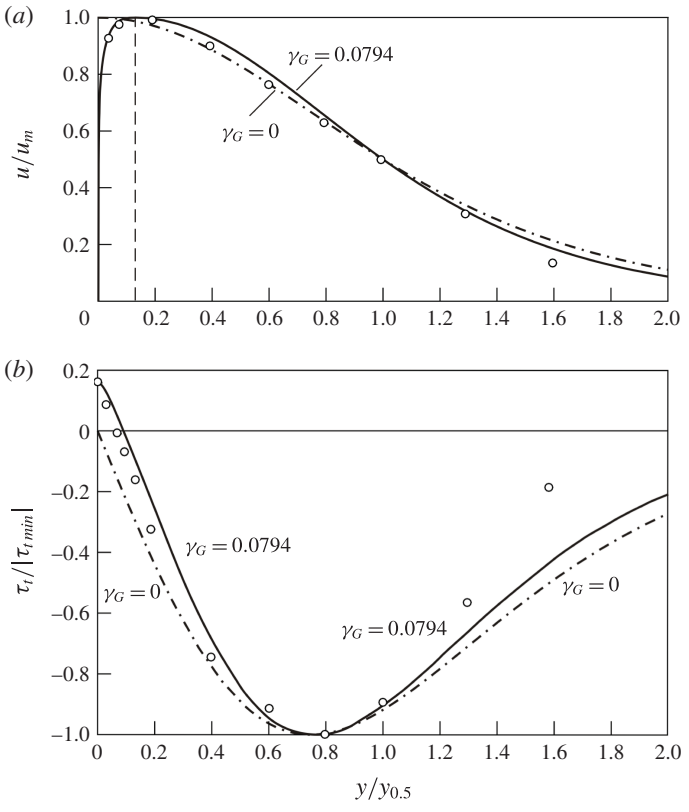

FIGURE 6. Distributions of velocity and shear stress at point II. —— $\gamma_G = 0.0794$, $Re_x = 2.1 \times 10^5$, after (9.1)–(9.4), ○ experiment, after Tailland & Mathieu (1967).

stress. Only if the second-order disturbances are taken into account does the shear stress have a finite value at the wall.

In figure 6 the special case $\gamma_G = 0.0794$ is plotted and compared with the limiting curve $\gamma_G = 0$. Obviously, the comparisons between the analytical results and the experimental data in figures 2–6 make the hypothesis $K_\infty \neq 0$ plausible. A definitely convincing verification, however, will be possible in the future, preferably by direct numerical solutions of turbulent wall jets.

Acknowledgements

I would like to thank Mrs G. Odemar and Professor Dr-Ing. H.-D. Papenfuß for their valuable assistance in the struggle to feed the computer with formulae and figures.

Appendix A. Function $G(\Lambda; D, E)$

The following implicit equation for the function $\gamma(Re)$ is considered:

$$\frac{1}{\gamma} = \frac{1}{\kappa} \ln(\gamma^n Re) + \hat{D} + \hat{E}\,\gamma. \tag{A 1}$$

In addition to the Kármán constant κ the equation contains three further constants: n, $\hat{D}$ and $\hat{E}$. One can find this equation quite often in the context of the theory of

turbulent shear flows near walls at high Reynolds numbers. The explicit solution of (A 1) is

$$\gamma = \frac{\kappa}{\ln Re}\, G(\Lambda;\ D,\ E) \tag{A 2}$$

where

$$\Lambda = \frac{2}{n}\ln Re, \quad D = 2\ln\left(\frac{2\kappa}{n}\right) + \frac{2\kappa}{n}\hat{D}, \quad E = \left(\frac{2\kappa}{n}\right)^2 \hat{E}. \tag{A 3a–c}$$

The function $G(\Lambda;\ D,\ E)$ has been defined and tabulated by Gersten & Herwig (1992). It satisfies the implicit algebraic equation

$$\frac{\Lambda}{G} + 2\ln\frac{\Lambda}{G} - D = \Lambda + E\,\frac{G}{\Lambda}, \tag{A 4}$$

which is independent of κ and n. The asymptote for $\Lambda \to \infty$ is

$$\begin{aligned} G(\Lambda\to\infty;\ D,\ E) \ =\ & 1 + \frac{1}{\Lambda}\,[2\ln\Lambda - D] + \frac{1}{\Lambda^2}\,[\,4\ \ln^2\Lambda - 4(1+D)\ln\Lambda \\ & + D^2 + 2\,D - E\,] + O(\Lambda^{-3}). \end{aligned} \tag{A 5}$$

Again for $\Lambda \to \infty$ the following integral has a rather simple solution:

$$\int_{\Lambda}^{\infty} \frac{G^2}{\Lambda^2}\,\mathrm{d}\Lambda = \frac{G}{\Lambda} + \left(\frac{G}{\Lambda}\right)^2 + O(\Lambda^{-3}). \tag{A 6}$$

Appendix B. Comment on the investigation by George *et al.* (2000)

In the introduction of my paper it has been stated that the analysis by George *et al.* refers to plane turbulent wall jets emerging from a wall perpendicular to the jet. This statement has been based on the following facts: firstly, figure 1 in George *et al.* shows a wall jet of this kind. Secondly, practically all experiments quoted in that investigation refer to wall jets emerging from a perpendicular wall. Thirdly, it is assumed in that investigation that $y_m/y_{0.5} = 0.17$ (table 1 in George *et al.* (2000)). This is an arbitrary unproven assumption which forces K_∞ to become zero.

Since the present analysis explicitly does not apply to wall jets emerging from a perpendicular wall, the investigation by George *et al.* has not been given further consideration in the present work.

If, however, one were to assume that the analysis of George *et al.* comprises also wall jets in the absence of a perpendicular wall, then two different asymptotic analyses are the consequence. Each asymptotic analysis is based on a different though unproven assumption (hypothesis). In George *et al.* it is assumed that $y_m/y_{0.5} = 0.17$, which leads to $K_\infty = 0$. In contrast, in the present analysis it is assumed that $K_\infty \neq 0$ with the consequence that $y_m/y_{0.5}$ tends to zero when the Reynolds number tends to infinity. Another fundamental difference between the two analyses exists concerning the effect of the inflow momentum flux K_j $(= M_0)$. In George *et al.* the Reynolds number is built with M_0 and hence all asymptotic formulae depend on M_0. In contrast to this, in the present work the asymptotic formulae are by definition independent of the inflow values M_0, U_0 and b (= slot width).

As has been mentioned above, it is hoped that direct numerical simulations will lead to a clarification at some future date.

REFERENCES

ABRAHAMSSON, H., JOHANSSON, B. & LÖFDAHL, L. 1994 A turbulent plane two-dimensional wall jet in a quiescent surrounding. *Eur. J. Mech. (B/Fluids)* **13**, 533–556.

BARENBLATT, G. I., CHORIN, A. J. & PROSTOKISHIN, V. M. 2005 The turbulent wall jet: a triple-layered structure and incomplete similarity. *Proc. Natl Acad. Sci. USA* **102** (25), 8850–8853.

BRADSHAW, P. & GEE, M. Y. 1960 Turbulent wall jets with and without an external stream. *Aero. Res. Counc. R&M* 3252.

GEORGE, W. K., ABRAHAMSSON, H., ERIKSSON, J., KARLSSON, R. I., LÖFDAHL, L. & WOSNIK, M. 2000 A similarity theory for the turbulent plane wall jet without external stream. *J. Fluid Mech.* **425**, 367–411.

GERSTEN, K. & HERWIG, H. 1992 *Strömungsmechanik. Grundlagen der Impuls-, Wärme- und Stoffübertragung aus asymptotischer Sicht*. Vieweg.

HAMMOND, G. P. 1982 Complete velocity profile and 'optimum' skin friction formulas for the plane wall jet. *Trans. ASME J. Fluids Engng* **104**, 59–65.

KARLSSON, R., ERIKSSON, J. & PERSSON, J. 1993 LDV measurements in a plane wall jet in a large enclosure. In *Laser Techniques and Applications in Fluid Mechanics* (ed. R. Adrian, D. Durâo, F. Durst, M. Heitor, M. Maeda & J. Whitelaw), pp. 311–332. Springer.

LAUNDER, B. E. & RODI, W. 1981 The turbulent wall jet. *Prog. Aerosp. Sci.* **19**, 81–128.

LAUNDER, B. E. & RODI, W. 1983 The turbulent wall jet – measurements and modeling. *Annu. Rev. Fluid Mech.* **15**, 429–459.

MYERS, G. E., SCHAUER, J. J. & EUSTIS, R. H. 1963 Plane turbulent wall jet flow development and friction factor. *Trans. ASME J. Basic Engng* **85**, 47–54.

NARASIMHA, R., NARAYAN, K. Y. & PARTHASARATHY, S. P. 1973 Parametric analysis of turbulent wall jets in still air. *Aeronaut. J.* **77**, 355–359.

POPE, S. B. 2000 *Turbulent Flows*. Cambridge University Press.

SAFFMAN, P. G. 1970 A model for inhomogeneous turbulent flow. *Proc. R. Soc. Lond.* A **317**, 417–433.

SCHLICHTING, H. & GERSTEN, K. 2003 *Boundary-Layer Theory*, 8th revised and enlarged edn. Springer.

SCHNEIDER, W. 1985 Decay of momentum flux in submerged jets. *J. Fluid Mech.* **154**, 91–110.

SCHNEIDER, W. 1991 Boundary-layer theory of free turbulent shear flows. *Z. Flugwiss. Weltraumforsch.* **15**, 143–158.

SCHNEIDER, M. E. & GOLDSTEIN, R. J. 1994 Laser Doppler measurement of turbulence parameters in a two-dimensional plane wall jet. *Phys. Fluids* **6**, 3116–3129.

SCHNEIDER, W. & MÖRWALD, K. 1987 Asymptotic analysis of turbulent free shear layers. In *Proc. Int. Conf. Fluid Mech.*, pp. 50–55. Beijing University Press.

TAILLAND, A. & MATHIEU, J. 1967 Jet pariétal. *J. Méc.* **6**, 103–130.

TOLLMIEN, W. 1926 Berechnung turbulenter Ausbreitungsvorgänge. *Z. Angew. Math. Mech.* **6**, 468–478; NACA TM 1085 (1945).

WYGNANSKI, I., KATZ, Y. & HOREV, E. 1992 On the applicability of various scaling laws to the turbulent wall jet. *J. Fluid Mech.* **234**, 669–690.